Saudi Pharmaceutical Journal 31 (2023) 101688

HOSTED BY

Contents lists available at ScienceDirect

Saudi Pharmaceutical Journal

journal homepage: www.sciencedirect.com

Original article

Synthesis, molecular structure and urease inhibitory activity of novel *bis*-Schiff bases of benzyl phenyl ketone: A combined theoretical and experimental approach

Rashid Ahmad [a,b], Momin Khan [b,*], Aftab Alam [a], Ahmed A. Elhenawy [c], Abdul Qadeer [d], Abdullah F. AlAsmari [e], Metab Alharbi [e], Fawaz Alasmari [e], Manzoor Ahmad [a,*]

[a] *Department of Chemistry, University of Malakand, P.O. Box 18800, Dir Lower, Khyber Pakhtunkhwa, Pakistan*
[b] *Department of Chemistry, Abdul Wali Khan University, Mardan 23200, Khyber Pakhtunkhwa, Pakistan*
[c] *Chemistry Department, Faculty of Science, Al-Azhar University, Cairo, Egypt*
[d] *Key Laboratory of Photonic and Electronic Bandgap Materials, Ministry of Education, College of Chemistry and Chemical Engineering, Harbin Normal University, Harbin 150025, China*
[e] *Department of Pharmacology and Toxicology, College of Pharmacy, King Saud University, Riyadh 11451, Saudi Arabia*

ARTICLE INFO

Article history:
Received 31 May 2023
Accepted 19 June 2023
Available online 24 June 2023

Keywords:
Bis-Schiff bases
Urease inhibition
Structure activity relationship
DFT
Molecular docking

ABSTRACT

Background: Urease belongs to the family of amid hydrolases with two nickel atoms in their core structure. On the basis of literature survey, this research work is mainly focused on the study of *bis*-Schiff base derivatives of benzyl phenyl ketone nucleus.
Objective: Synthesis of benzyl phenyl ketone based *bis*-Schiff bases in search of potent urease inhibitors.
Method: In the current work, *bis*-Schiff bases were synthesized through two steps reaction by reacting benzyl phenyl ketone with excess of hydrazine hydrate in ethanol solvent in the first step to get the desired hydrazone. In last, different substituted aromatic aldehydes were refluxed in catalytic amount of acetic acid with the desired hydrazone to obtain *bis*-Schiff base derivatives in tremendous yields. Using various spectroscopic techniques including FTIR, HR-ESI-MS, and ^{1}H NMR spectroscopy were used to clarify the structures of the created *bis*-Schiff base derivatives.
Results: The prepared compounds were finally screened for their *in-vitro* urease inhibition activity. All the synthesized derivatives (**3**–**9**) showed excellent to less inhibitory activity when compared with standard thiourea (IC_{50} = 21.15 ± 0.32 μM). Compounds **3** (IC_{50} = 22.21 ± 0.42 μM), **4** (IC_{50} = 26.11 ± 0.22 μM) and **6** (IC_{50} = 28.11 ± 0.22 μM) were found the most active urease inhibitors near to standard thiourea among the synthesized series. Similarly, compound **5** having IC_{50} value of 34.32 ± 0.65 μM showed significant inhibitory activity against urease enzyme. Furthermore, three compounds **7, 8,** and **9** exhibited less activity with IC_{50} values of 45.91 ± 0.14, 47.91 ± 0.14, and 48.33 ± 0.72 μM respectively. DFT used to calculate frontier molecular orbitals including; HOMO and LUMO to indicate the charge transfer from molecule to biological transfer, and MEP map to indicate the chemically reactive zone suitable for drug action. The electron localization function (ELF), non-bonding orbitals, AIM charges are also calculated. The docking study contributed to the analysis of urease protein binding.

1. Introduction

The creation of carbon nitrogen double bond plays a significant role in the synthesis of organic compounds. Schiff bases can be synthesized in acidic as well as in basic media through the reaction of primary amines with aldehydes or ketones (Upadyaya et al., 2018, Ullah et al., 2020, Rahim et al., 2020). Azomethine or imine groups are present in a variety of synthetic or naturally occurring substances (Alam et al., 2022b, Okoli and Modise, 2018). Due to their broad biological potential, Schiff bases and di-imines/*bis* Schiff bases have gained importance in past few years. These compounds are often made by the condensation of aliphatic or aromatic aldehydes with aniline/aliphatic amines in the company of acid or base in catalytic amount (Nasli-Esfahani et al., 2019, Yu et al., 2022).

* Corresponding authors.
E-mail addresses: Mominkhan@awkum.edu.pk (M. Khan), Manzoorahmad@uom.edu.pk (M. Ahmad).

https://doi.org/10.1016/j.jsps.2023.06.021
1319-0164/

Bis-Schiff bases or azines are compounds containing two carbon nitrogen double bonds in its structures with general formula ($R_1HC{=}N{-}N{=}CHR_2$) (Figueredo et al., 2019, Khan et al., 2018, ABDELMADJID et al., 2021, Alam et al., 2022a). Azines may be symmetric ($R_1R_2 = R_3R_4$) or asymmetric ($R_1R_2 \neq R_3R_4$), and depend on the nature of the attached substituents (R). Amongst other compounds, *bis*-Schiff bases received greater attention due to their various biological activities like anti-oxidant, anti-tumour, anti-bacterial, anti-proliferative, anti-convulsant and anti-parasitic (Arshad et al., 2020, Zhong et al., 2006, Khan et al., 2009, Yapar et al., 2022, Al-Mudhafar et al., 2022). A number of *bis*-Schiff base derivatives have been reported by synthetic or medicinal chemists such as, Alam *et al* had been reported the synthesis of *bis*-Schiff base derivatives of 4-nitroacetophenone and screened them for their *in vitro* α-glucosidase inhibitory activity with excellent results (Alam et al., 2022a). Similarly, benzimidazole based *bis*-Schiff base derivatives have been synthesized and evaluated for α-glucosidase activity by Rahim and his colleagues (Rahim et al., 2020). On the other hand, Khan *et al* reported the synthesis of isatin *bis*-Schiff base derivatives and tested them for anti-glycating activity which showed potent activity (Khan et al., 2009) **(**Fig. 1**)**.

Amid hydrolase family includes urease, which has two nickel atoms at the centre of its core structure (Ahmad et al., 2022). The hydrolysis of urea into ammonia (NH_3) and carbon dioxide (CO_2) is stimulated by this enzyme. High urease activity causes the stomach overly alkaline or basic, that encourages the endurance of bacteria (Helicobacter pylori), which in turn causes the growth of digestive and stomach abscesses, which can ultimately result in cancer (Ahmed et al., 2017, Sudkolai and Nourbakhsh, 2017). The activity of urease regulates the metabolism of nitrogen in cows and further beasts. Since these enzymes aid in some bacterial pathogens' survival, a significant increase in their level can result in a number of diseases (Kafarski and Talma, 2018, Cantarella et al., 2018). Additionally, raised ammonia levels disrupt some metabolic processes and harm GIT epithelial cells (Domínguez et al., 2008). Many different types of compounds, including hydroxamic derivatives, phosphodiamideates, and thiolates destined to nickel atom of the enzyme, and a little peptide chains with a ligand that may chelate with nickel of urease, have been reported as urease inhibitors (Kosikowska and Berlicki, 2011, Soares et al., 2012). Finding new urease inhibitors with low toxicity, outstanding steadiness, and bio-availability is essential because these compounds have unfavourable side effects (Silva et al., 2017).

2. Experimental

2.1. Chemistry

All the solvents, reagents, and chemicals (Benzyl Phenyl Ketone CAS No: 451–40-1) used in this research work were of analytical grade (98–99 % pure) and purchased from Sigma Aldrich, TCI, BDH, and Merck. The masses of the created compounds were determined using cutting-edge high resolution electrospray ionization mass spectrometry (HR-ESI-MS) technology (Agilent 6530 LC Q-TOF, USA/EU, produced in Singapore). ^{1}H NMR experiments were performed in $CDCl_3$ using Avance Bruker AM 400-MHz spectrophotometer and IR spectra were recorded on Jasco FT-IR47700 spectrometer. The following splitting patterns are used: singlet (s), doublet (d), double doublet (dd), triplet (t), and multiplet (m). Coupling constant (*J*) is supplied in Hz and chemical shift is stated in ppm. Thin layer chromatography (TLC) was used to keep track of how each reaction was progressing which was performed on pre-coated silica gel aluminum plates (Kieselgel 60, 254, E. Merck, Germany). The Chromatograms were visualized by ultraviolet light at 254 and 365 nm. The titled compounds were synthesized and characterized satisfactorily.

2.1.1. General procedure for the compounds synthesis (2–9)

1,2-diphenylethylidene hydrazine **(2)** was produced in a 100 ml round-bottomed flask by refluxing benzyl phenyl ketone with excess hydrazine hydrate while maintaining continual stirring for

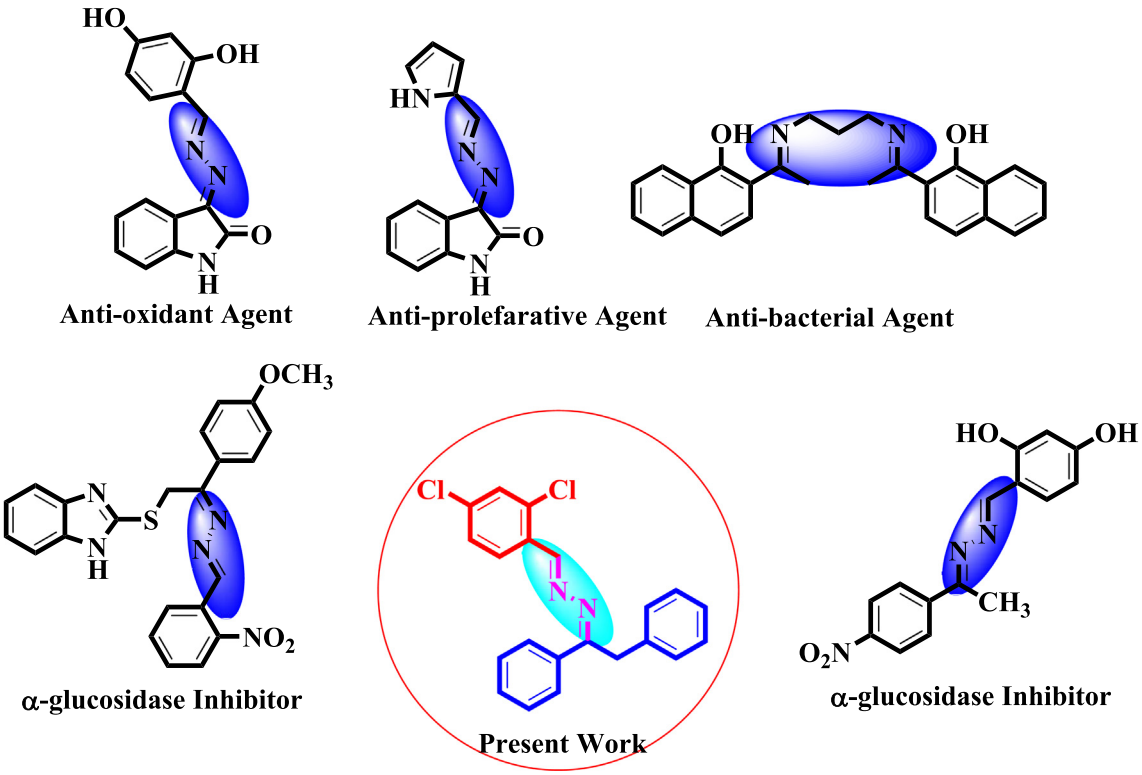

Fig. 1. *Bis*-Schiff bases having various biological activities.

3 to 4 h in distilled methanol and acetic acid as catalyst. After the reaction was finished, a white precipitate of the product was produced. Utilizing thin layer chromatography in a 20% solvent system of *n*-hexane and ethyl acetate, the reaction's completion was seen. After reaching room temperature, the reaction liquid was decanted into a beaker filled with ice cubes. To get a pure product, the resulting chemical was recrystallized with pure methanol.

In second step, different aromatic substituted aldehydes were refluxed with 1,2-diphenylethylidene hydrazine **(2)** in the existence of acetic acid as a catalyst in methanol for 3–5 hrs to get *bis*-Schiff base derivatives **(3–9)**. Progress of the reactions was checked with thin layer chromatography having solvent system of *n*-hexane and ethyl acetate (3:2). Following completion, these mixtures were poured onto cold distilled water. Precipitates were made, washed after filtration and collected. The structures of these derivatives were elucidated with the help of FTIR, ^{1}H NMR and HR-ESI-MS spectroscopy.

2.2. Spectral data of the synthesized compounds (3–9)

2.2.1. 1-(2,4-dichlorobenzylidene)-2-(1,2-diphenylethylidene) hydrazine (3)

White Powder; Yield: 87 %; M.P: 210–211 °C; FTIR: υ/cm^{-1}: 3007, 2923, 2856, 1583, 1463, 1099, 948, 767. ^{1}H NMR (400 MHz, $CDCl_3$): δ (ppm) = 8.98 (s, Ar-H, 1H, =CH—), 8.16 (d, Ar-H, *J* = 8.4 Hz, 2H, H-5"), 7.89 (s, Ar-H, 1H, H-3"), 7.88 (d, Ar-H, *J* = 8.4 Hz, 1H, H-6"), 7.44–7.30 (m, Ar-H, 5H, H-2, H-3, H-4, H-5, H-6), 7.24–7.11 (m, Ar-H, 5H, H-2', H-3', H-4', H-5', H-6'), 4.34 (s, 2H, —CH_2); HRMS (ESI$^+$): $[M + H]^+$ calcd for $C_{21}H_{16}Cl_2N_2$: 366.0691; found 367.1076.

2.2.2. 1-(1,2-diphenylethylidene)-2-(4-nitrobenzylidene)hydrazine (4)

Yellow Powder; Yield: 86 %; M.P: 200–201 °C; FTIR: υ/cm^{-1}: 3009, 2925, 2854, 1685, 1649, 1595, 1450, 1340, 1284, 1103, 1024, 960, 842. ^{1}H NMR (400 MHz, $CDCl_3$): δ (ppm) = 8.69 (s, Ar-H, 1H, =CH—), 8.32 (d, Ar-H, *J* = 8.8 Hz, 2H, H-2", H-6"), 8.03 (d, Ar-H, *J* = 8.8 Hz, 2H, H-3", H-5"), 7.55–7.41 (m, Ar-H, 5H, H-2, H-3, H-4, H-5, H-6), 7.36–7.11 (m, Ar-H, 5H, H-2', H-3', H- 4', H-5', H-6'), 4.26 (s, 2H, —CH_2); HRMS (ESI$^+$): $[M + H]^+$ calcd for $C_{21}H_{17}N_3O_2$: 343.1321; found 344.1393.

2.2.3. 1-(1,2-diphenylethylidene)-2-(2-hydroxy-5-nitrobenzylidene) hydrazine (5)

Off White Powder; Yield: 83 %; M.P: 206–207 °C; FTIR: υ/cm^{-1}: 3290, 3030, 2931, 1683, 1598, 1446, 1336, 1276, 1188, 1074, 840. ^{1}H NMR (400 MHz, $CDCl_3$): δ (ppm) = 8.00 (m, 2H, =CH—, 4"), 7.53–7.42 (m, Ar-H, 2H, H-6", H-5), 7.37 (s, Ar-H, 1H, H-3"), 7.32–7.30 (m, Ar-H, 4H, H-2, H-3, H-4, H-6), 7.28–7.42 (m, Ar-H, 5H, H-2', H-3', H-4', H-5', H-6'), 4.12 (s, 2H, —CH_2); HRMS (ESI$^+$): $[M + H]^+$ calcd for $C_{21}H_{17}N_3O_3$: 359.1270; found 359.2439.

2.2.4. 1-(4-chlorobenzylidene)-2-(1,2-diphenylethylidene)hydrazine (6)

Yellowish Powder; Yield: 79 %; M.P: 165–166 °C; FTIR: υ/cm^{-1}: 3055, 2997, 2854, 1683, 1591, 1488, 1286, 1218, 1089, 960, 862. ^{1}H NMR (400 MHz, $CDCl_3$): δ (ppm) = 8.27 (s, Ar-H, 1H, =CH—), 7.88 (d, Ar-H, *J* = 7.2 Hz, 2H, H-2", H-6"), 7.64 (d, Ar-H, *J* = 7.2 Hz, 2H, H-3", H-5"), 7.55–7.42 (m, Ar-H, 5H, H-2, H-3, H-4, H-5, H-6), 7.39–7.13 (m, Ar-H, 5H, H-2', H-3', H-4', H-5', H-6'), 4.26 (s, 2H, —CH_2); HRMS (ESI$^+$): $[M + H]^+$ calcd for $C_{21}H_{17}ClN_2$: 333.1080; found 334.1155.

2.2.5. 1-(1,2-diphenylethylidene)-2-(4-(methylthio)benzylidene) hydrazine (7)

White Powder; Yield: 79 %; M.P: 177–178 °C; FTIR: υ/cm^{-1}: 3284, 2918, 2850, 1616, 1409, 1089, 1033, 860, 767. ^{1}H NMR (400 MHz, $CDCl_3$): δ (ppm) = 8.80 (s, Ar-H, 1H, =CH—), 7.99 (d, Ar-H, *J* = 7.2 Hz, 2H, H-3", H-5"), 7.87 (d, Ar-H, *J* = 7.2 Hz, 2H, H-2", H-6"), 7.72–7.20 (m, Ar-H, 9H, H-2, H-3, H-4, H-5, H-6, H-2', H-3', H-4', H-5', H-6'), 4.56 (s, 2H, —CH_2), 2.50 (s, 3H, -SCH_3), HRMS (ESI$^+$): $[M + H]^+$ calcd for $C_{22}H_{20}N_2S$: 344.1347; found 345.2031.

2.2.6. 1-(1,2-diphenylethylidene)-2-(4-methylbenzylidene)hydrazine (8)

Off White Powder; Yield: 80 %; M.P: 162–163 °C; FTIR: υ/cm^{-1}: 3007, 2918, 2850, 1620, 1512, 1460, 1176, 970, 817. ^{1}H NMR (400 MHz, $CDCl_3$): δ (ppm) = 8.69 (s, Ar-H, 1H, =CH—), 7.96 (d, Ar-H, *J* = 7.5 Hz, 2H, H-3", H-5"), 7.75 (d, Ar-H, *J* = 7.5 Hz, 2H, H-2", H-6"), 7.55–7.42 (m, Ar-H, 5H, H-2, H-3, H-4, H-5, H-6), 7.38–7.07 (m, Ar-H, 5H, H-2', H-3', H-4', H-5', H-6'), 4.54 (s, 2H, —CH_2), 2.39 (s, 3H, —CH_3), HRMS (ESI$^+$): $[M + H]^+$ calcd for $C_{22}H_{20}N_2$: 312.1626; found 313.0928.

2.2.7. 1-(1,2-diphenylethylidene)-2-(4-hydroxybenzylidene)hydrazine (9)

Yellowish Powder; Yield: 87 %; M.P: 176–177 °C; FTIR: υ/cm^{-1}: 3602, 3022, 1595, 1492, 1442, 1278, 1072, 1024. ^{1}H NMR (400 MHz, $CDCl_3$): δ (ppm) = 8.69 (s, Ar-H, 1H, =CH—), 7.89 (d, Ar-H, *J* = 7.5, 2H, H-3", H-5"), 7.34 (d, Ar-H, *J* = 7.5 Hz, 2H, H-2", H-6"), 7.24–7.12 (m, Ar-H, 9H, H-2, H-3, H-4, H-5, H-6, H-2', H-3', H-4', H-5', H-6'), 4.33 (s, 2H, —CH_2); HRMS (ESI$^+$): $[M + H]^+$ calcd for $C_{21}H_{18}N_2O$: 314.1419; found 314.1897.

2.3. Urease inhibition assay

According to the reported methodology, urease inhibitory activity was carried out (Rahim et al., 2020; Ritchie et al., 2011). Briefly, a 96-well plate containing 40 L of pH 6.8 phosphate buffer, 10 L of the synthesised derivatives, and 10 L of enzyme was incubated for 10 min at 37 °C. 40 L of phenol reagent and 40 L of alkali reagent solutions were added to each well. The experiment was carried out in three duplicates. The Microplate Reader (Bio-TekELx 800, Instruments, Inc., and USA) was used to read the absorbance at 625 nm. Thiourea was the usual inhibitor in this situation. Using the equation shown below, the percentage of inhibition was computed.

$$\%\text{Inhibition} = (\text{Absorbance Control} - -\text{Absorbance Sample})/\text{Absorbance Control} \times 100$$

2.4. Computational methodology

Density functional theory (DFT) calculations were performed using the Gaussian09 and Gaussview5 software tools to determine the optimal structures of **(3–9)** compounds (Frisch et al., 2010). The computations were performed using the 6-311G++ (d,p) higher order basis set and the B3LYP technique. The optimal structure carried out the geometrical parameters as well as other molecular characteristics like HOMO-LUMO, NBO, and MEP. An atom in Molecule (AIM) theory, which makes use of Multiwfn software, was used to calculate the topological parameters and the electron localization function. Furthermore, the following equations were used for the calculation of chemical indices including: global nucleophilicity μ, electrophilicity ω, chemical hardness η, based on electronic chemical potential φ, and maximum electron transfer ΔN_{max}.

$$\eta = 1/2\left[\partial^2 E/\partial^2 N^2\right]_{\upsilon(r)} = 1/2\left[\partial E/\partial N^2\right]_{\upsilon(r)} \quad (1)$$

$$S = 1/\eta \quad (2)$$

$$\mu = [\partial E/\partial N]_{\upsilon(r)} \quad (3)$$

$$\chi = -[\partial E/\partial N]_{\upsilon(r)} \quad (4)$$

$$\omega iVs = (I + A)2/4(I - A) \quad (5)$$

$$\Delta Nmax = \chi/2\eta \quad (6)$$

2.5. Molecular docking protocol

GOLD was used to conduct a docking investigation for the target molecules (version 5.2). After obtaining the crystallized urease structure, H_2O and inhibitors were taken out and H atoms were added. The examined ligands were redocked into the vacant active site after the standard inhibitor was removed from it. ChemPLP scoring function was generated for measuring the binding affinity and the charges were assigned with CHARMM force field. The structure with the lowest RMSD score was used to generate different ligand poses. For calculating the binding affinity, the ChemPLP scoring function was created, and the CHARMM force field was used to assign charges. To create several ligand postures, the structure with the lowest RMSD score was selected.

2.6. Molecular dynamic

Calculations of molecules were made with molecular dynamic calculations. The Binding free energy, Vander Waals energy, electrostatic energy, kinetic energy and potential energy changes of the studied molecules were deliberate for these calculations. In addition, this study examined the interactions between molecules and the 4UBP protein. These interaction energies were investigated in the period between 0 ns and 250 ns. As a result of the interaction of the three molecules studied with the protein, the values of the binding free energy change were calculated. This calculation is given in equation (7).

$$\Delta G_{Bind} = G_{complex} - (G_{res} + G_{lig}) \quad (7)$$

In the above equation, ΔG_{Bind} gives the total binding free energy value between the ligand and the protein. G_{lig}, G_{res}, and $G_{complex}$ values in the equation are the values of the ligand molecule, urease receptor protein, and complex molecule, respectively (Irfan et al., 2023).

3. Results

3.1. Chemistry

Continuing our efforts to discover potent inhibitors of urease enzyme, we successfully synthesized fourteen *bis*-Schiff base derivatives based on benzyl phenyl ketone **(1)** through two step reactions. Initially, benzyl phenyl ketone **(1)** was refluxed with excess of hydrazine hydrate in methanol solvent in containing 4–6 drops acetic acid (catalyst) for 3–4 hrs to get the desired 1,2-diphenylethylidene hydrazine **(2)** in excellent yield. Then, different aromatic benzaldehydes were refluxed with 1,2-diphenylethylidene hydrazine **(2)** in the company of acetic acid in catalytic quantity to obtain various *bis*-Schiff base derivatives **(3–9)** (Scheme 1). The synthesized derivatives were confirmed with the help of FTIR, HR-ESI-MS and ^{1}H NMR spectroscopy and lastly screened them for their *in-vitro* urease inhibitory activity. The synthesised derivatives' ^{1}H NMR spectrum exposed indications for methyl (—CH_3), methylene (—CH_2), and multiple methine (—CH—) protons. Signals that resonated at δ 11.6–11.2 in the down field area of the spectrum were caused by the presence of —OH protons. Similar to this, in the spectrums signals appeared at δ 8.69 to 6.90 were caused by aromatic protons, whereas signals seen in the up field region δ 3.12–3.14 and 2.39–2.30 of the spectrums were caused due to the presence of methylene and methyl protons respectively. Additionally, HR-ESI-MS spectra were used to confirm the compounds' molar masses. The experimental part contains a detailed spectrum interpretation of the synthesized derivatives.

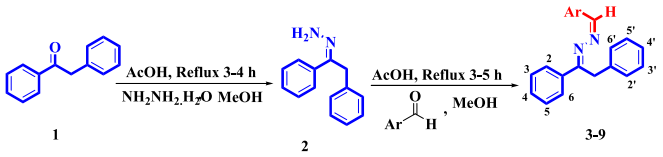

Scheme 1. Preparation of *bis*-Schiff base derivatives of benzyl phenyl ketone (**3–9**).

3.2. In-Vitro urease inhibitory activity

After structural confirmation of the prepared analogues through FTIR, HR-ESI-MS and ^{1}H NMR spectroscopy, they were tested for their urease inhibitory activity (*in-vitro)*. The whole derivatives presented excellent to good inhibition activity in the range of IC_{50} values of 22.21 ± 0.42 to 47.91 ± 0.14 μM when compared with standard thiourea (IC_{50} = 21.15 ± 0.32 μM). Compounds **3** (IC_{50} = 22.21 ± 0.42 μM), **4** (IC_{50} = 26.11 ± 0.22 μM) and **6** (IC_{50} = 28.11 ± 0.22 μM) were found the most active urease inhibitors near to standard thiourea among the synthesized series. Similarly, compound **5** having IC_{50} value of 34.32 ± 0.65 μM was showed significant inhibitory activity against urease enzyme. Furthermore, three compounds **7, 8,** and **9** exhibited less activity with IC_{50} values of 45.91 ± 0.14, 47.91 ± 0.14, and 48.33 ± 0.72 μM respectively (Table 1).

4. Discussions

4.1. Structure activity relationship study

To ascertain the effect of the substituted aromatic ring (Ar-group) on the inhibition of the anti-oxidant activity, a rigorous structure activity relationship (SAR) was carried out. To illuminate our outcomes, we combined the mark molecules into a fictitious Ar-group with several substituted benzaldehydes attached at either the same or different positions. Three compounds **3, 4,** and **6** among the synthesized analogues attributed excellent inhibitory activity in the range of IC_{50} values of 22.21 ± 0.42 to 28.11 ± 0.22 μM near to thiourea as standard (IC_{50} = 21.15 ± 0.32 μM). The top activity of compound **3** could be due to the occurrence of electron withdrawing two chlorine groups attached to the benzene ring at *ortho* and *para* position. A decrease occurs in the activity of compound **6** (IC_{50} = 28.11 ± 0.22 μM) might be due to the removal of one chlorine atom from the *ortho* position of the benzene ring. Similarly, comparing compound **4** (IC_{50} = 26.11 ± 0.22 μM) with **5** (IC_{50} = 34.32 ± 0.65 μM), the excellent activity of compound **4** could be due to the attachment of electron withdrawing nitro group at *para* position of the benzene ring while the decrease occurs in the activity of compound **5** may be due to the change in position of nitro group from *para* to *meta* and attachment of hydroxyl group at *para* position of the benzene ring (Fig. 2). On the other hand, by comparing compound **8** (IC_{50} = 45.91 ± 0.14 μM), **9** (IC_{50} = 47.91 ± 0.14 μM), and **7** (IC_{50} = 48.33 ± 0.72 μM), the less activities of the compounds may be due to the attachment of electron donating groups attached at *para* position of the benzene ring. Because the strength of the attached Ar-groups showed only slight variations in their ability to inhibit urease, the structure activity relationship studies explore the crucial role of these groups in urease inhibition.

Table 1
Urease inhibition potential (in-vitro) of the synthesized *bis*-Schiff base derivatives **(3–9)**.

C. No	Structure	IC_{50} (μM) ± SEM	C. No	Structure	IC_{50} (μM) ± SEM
3	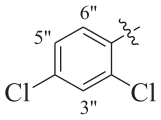	22.21 ± 0.42	**7**	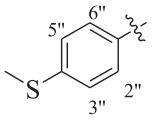	48.33 ± 0.72
4	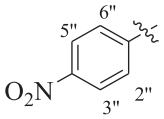	26.11 ± 0.22	**8**	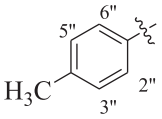	45.91 ± 0.14
5	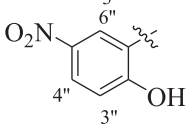	34.32 ± 0.65	**9**	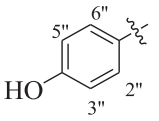	47.91 ± 0.14
6	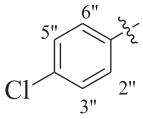	28.11 ± 0.22	**Thiourea**		21.15 ± 0.32

SEM = standard error mean.

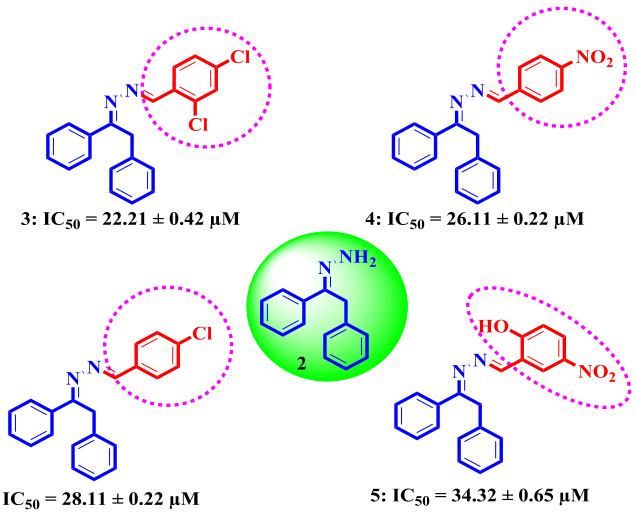

Fig. 2. The most effective compounds of the series.

4.2. Global DFT reactivity indices in the ground state

Conceptual density functional theory (DFT) can be used to know the reactivity of chemical reactions. The analysis of reactivity indices, such as the global reactivity index (GRI) and the local reactivity index (LRI) is an important aspect of such theories. These reactivity indices allow researchers to analyse the variations of chemical reactivity in different reactions and can be used to predict the most reactive pathways for a given reaction and underlying mechanism of a chemical reaction and thus design better synthetic strategies. The used universal directories including global nucleophilicityμ, electrophilicity ω, chemical hardness η, and electronic chemical potential φ, for seven investigated molecules **(3–9)** (Table 2).

The electrophilicity index arranged as **5 > 7 > 6 > 9 > 8 > 4 > 3**. Furthermore, Δε was capable to conclude a molecule's kinetic stability. Molecule **3** is highest Δε and η than other compounds **4–9** about 0.2–0.8 eV, at the same time **3** is highest softness than other compounds and is more kinetically stable than **4–9**, these lead to higher kinetic stability for **3** (Costa et al., 2017). Furthermore, the antioxidant effect is related to a low value of chemical potential (Domingo). The lowest electronic chemical potential belong to molecule **5** (φ = −3.11 eV), which lower than that other compounds **3, 4,** and **6–9**, with a difference of about between 0.5 eV and 0.9 eV. This indicates that molecule **5** has a higher tendency to donate electrons and may enhance the activity of the hybrids **(3–9)**.

4.3. Homo-LUMO and electrostatic potential map MEP

A significant influence is played by the lowest unoccupied molecular orbital (LUMO) and the highest occupied molecular orbital (HOMO) in determining the chemical behaviour of a molecule. HOMO and LUMO are shifted along **(3–9)** molecular skeletons (Fig. 3). The plot of HOMO and LUMO orbitals shows that the molecule's positive and negative regions are distributed throughout **(3–9)**. The detecting active site for receptor is explained by the charge transfer interaction between the molecules, which is determined by the energy gap between LUMO and HOMO. A small energy gap indicating the easy charge transfer between the two orbitals and high charge transfer contact, explaining the selective inhibition for **(3–9)** investigated molecules.

MEP is a marker for the distribution and polarisation of the outer electrons in connection to the reactivity and capacity of the molecular environment to interact with H-atoms. It also offers comprehensive details on the locations of electrophilic and nucleophilic chemicals. Because the polar ("-"charge is represented by red color) and nonpolar ("+"charge is represented by blue color) molecular zones are distinguished in Fig. 4, we may graphically calculate the statistical polarity. It was discovered that the green area had potential that was midway between the dual red and blue. As the distribution of colours on MEP changes due to electrostatic potential levels, red, yellow, blue, and green appear in increasing order. The examined compounds **(3–9)** ability to bind with biological enzymes based on size and shape was supported by the electron distribution. Fig. 4 showed that the red region encompassing the =N—N=, which increased the effect of electrophilicity**.**

4.4. Hole density distribution and electron excitation analysis

The distribution of electron and hole density provides the concept of multi-molecular orbital excitation, which delivers clear

Table 2
TD-DFT/6–311++G(d,p) electronic-chemical indices "Electronic chemical potential φ, Chemical hardness η, global electrophilicity ω and global nucleophilicity μ".for the reagents elaborate in the reaction under investigation in vacuum at 25 °C.

Species	HOMO	LUMO	Δε	η	S	φ	μ	ω	ΔN_{max}
3	−5.345	−2.087	3.257	1.629	0.614	−3.716	4.239	10.336	−1.141
4	−5.551	−2.078	3.473	1.736	0.576	−3.815	4.190	10.287	−1.098
5	−4.934	−1.288	3.646	1.823	0.549	−3.111	2.655	6.866	−0.853
6	−5.414	−1.932	3.482	1.741	0.574	−3.673	3.874	9.585	−1.055
7	−6.618	−1.419	5.199	2.600	0.385	−4.018	3.106	8.220	−0.773
8	−5.475	−2.042	3.432	1.716	0.583	−3.759	4.116	10.111	−1.095
9	−5.431	−2.013	3.419	1.709	0.585	−3.722	4.052	9.965	−1.089

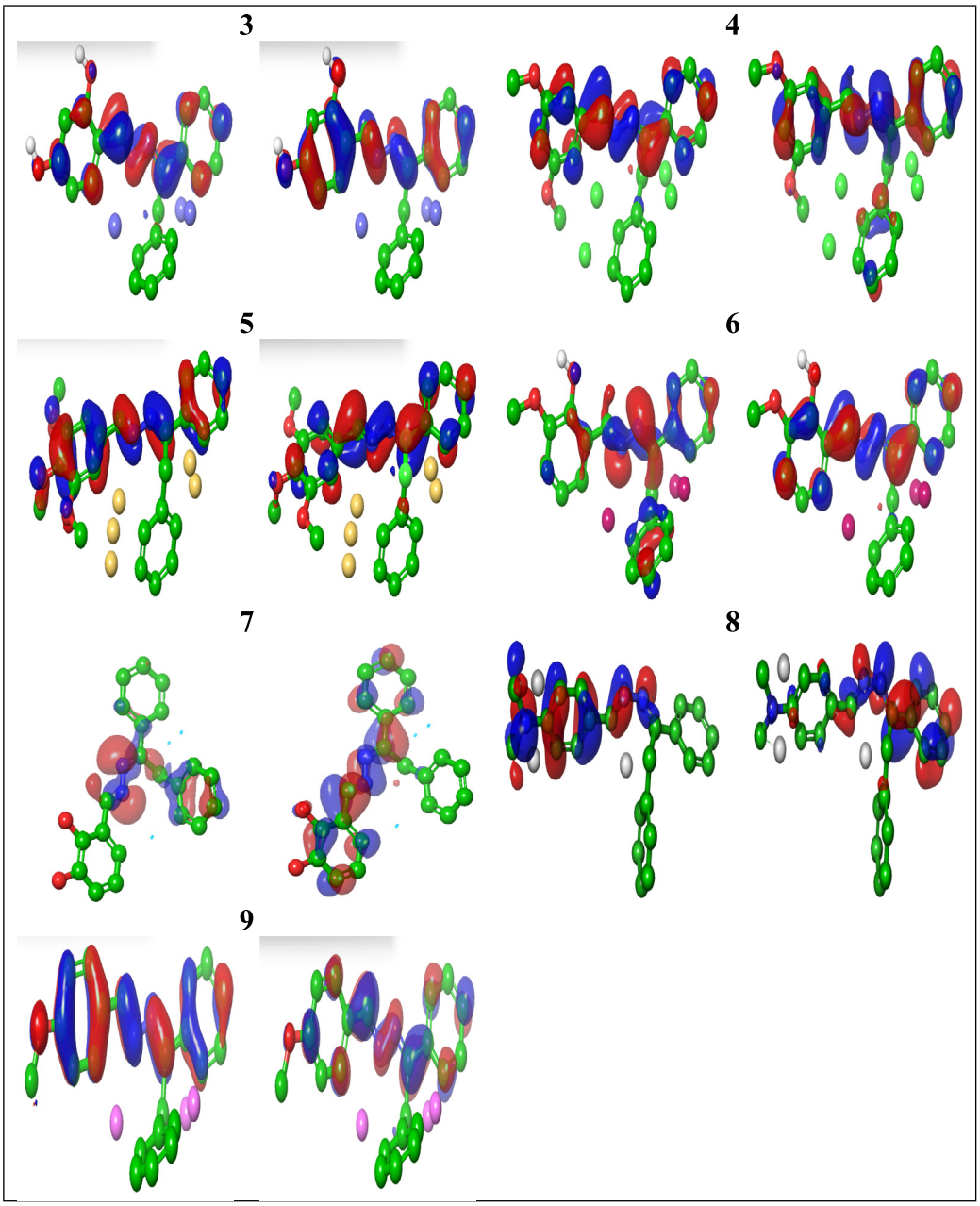

Fig. 3. HOMO / LUMO map for compounds **(3–9)** at *TD-DFT/6–311++G(d,p)*.

features of the excited state for the receptors and their corresponding receptor anions. One can learn more about the electrical structure and characteristics of **(3–9)** molecules by evaluating the electron and overall density distribution. Understanding the mechanism of molecular recognition and binding in receptor-ligand and metal–ligand systems is made possible by the information provided. The excitation of an electron from an occupied to virtual molecular orbital (MO) is employed as a model for the excited state

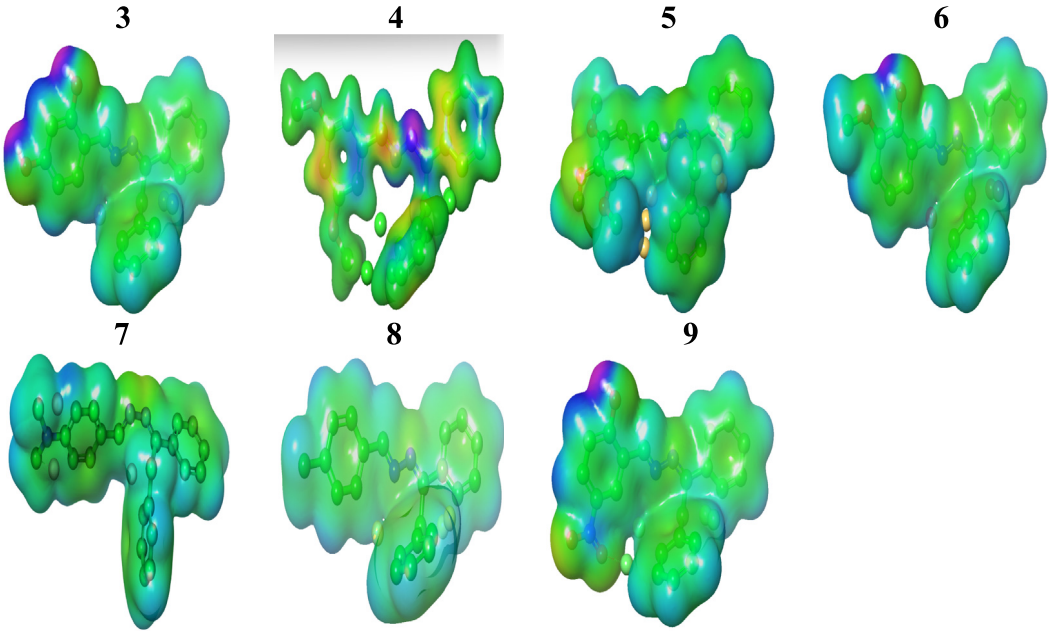

Fig. 4. MEP map for compounds **(3–9)** at *TD-DFT/6–311++G(d,p).*

when an electron is delocalized from A to B as part of a single electron excitation process. One can learn more about the characteristics of the excited state by contrasting it with the ground state MO and the various regions of photo-excited states that are shown by electron density distribution maps. These maps of the electron density distribution illustrate the geographical distribution of the electron density within the molecule and can reveal details about the energy level of the excited state, the location and kind of excited electrons, and the level of electron delocalization.

In Fig. 5, EDD map exhibits a thicker surface on the entire diphenylethylidene-hydrazine fragments for seven investigated compounds **(3–9)**, indicating a higher electron density in those regions. On the other hand, the HDD map displays a denser surface on the entire =N—N= fragment, indicating a higher hole density.

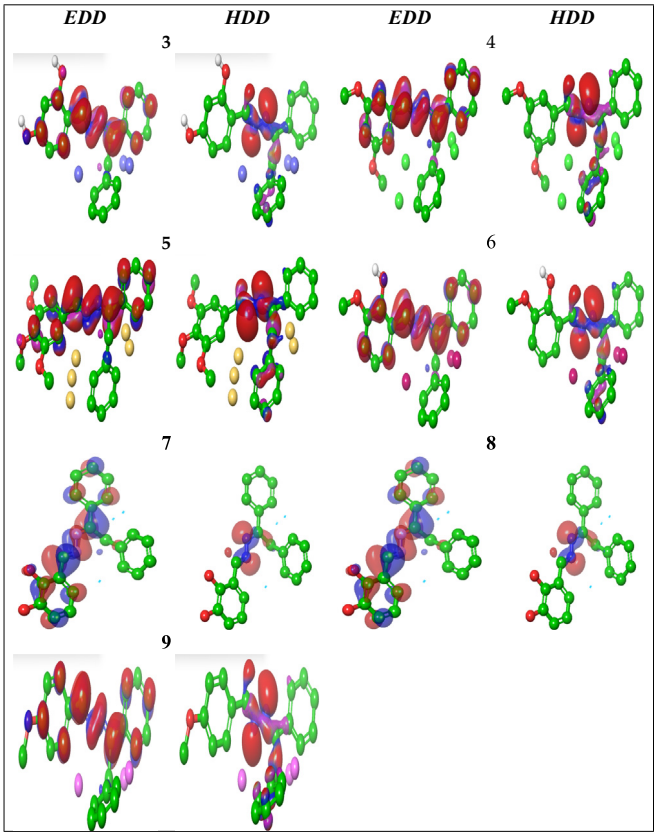

Fig. 5. EDD and HDD profile for the excited state for compounds **(3–9)**.

4.5. Topology analysis

The nature of the intramolecular interactions in the seven molecules **(3–9)** was investigated using topological analysis of the atoms in the molecule (Fig. 6). According to Atoms in Molecule (AIM) analysis the presence of bond critical path (BCP) as white, blue, yellow, green and red dots, that ensures that the bond between the atoms, which represented dots. Fig. 7 showed formed RCP between C19•••O27 and C13•••C25 at compounds **3, 4 and 9**; C9•••O21, NO8•••C20 and C17•••F27 at compound **5**; C6•••C18 and C14•••C24 at compounds **6** and **8**; N10•••C15 and C19•••C25 at compound **7**. The total electron density $p_{(r)}$ and Laplacian ($\nabla^2 p_{(r)}$) describe the nature of bonds. Total electron density is given by the expression, $\frac{1}{4}\nabla^2 p_{(r)} = G(r) + \gamma\{r\}$ where G(r) and V (r) are Lagragian kinetic energy and potential energy densities at critical points, respectively. The values$\nabla^2 p_{(r)}$ > 0 and G(rBCP) + V (rBCP) > 0, that indicate that the bond is a weak bond. Ratio of G(r BCP)/V(r BCP) indicates that the hydrogen bond has a non-covalent nature (Lu and Chen, 2012).

4.6. Non-covalent interactions (NCI)

The structures of synthesized seven molecules **(3–9)** are influenced by several types of interactions, including covalent, non-covalent, and electrostatic interactions. Reduced Density Gradient (RDG) analysis can reveal Non-Covalent interactions (NCI), and visualize those using isosurfaces with logradients depending on how strong the interaction is. Several ligand postures were generated using the west RMSD score. Sign (λ_2) values give information about the sort of bonding, with large negative

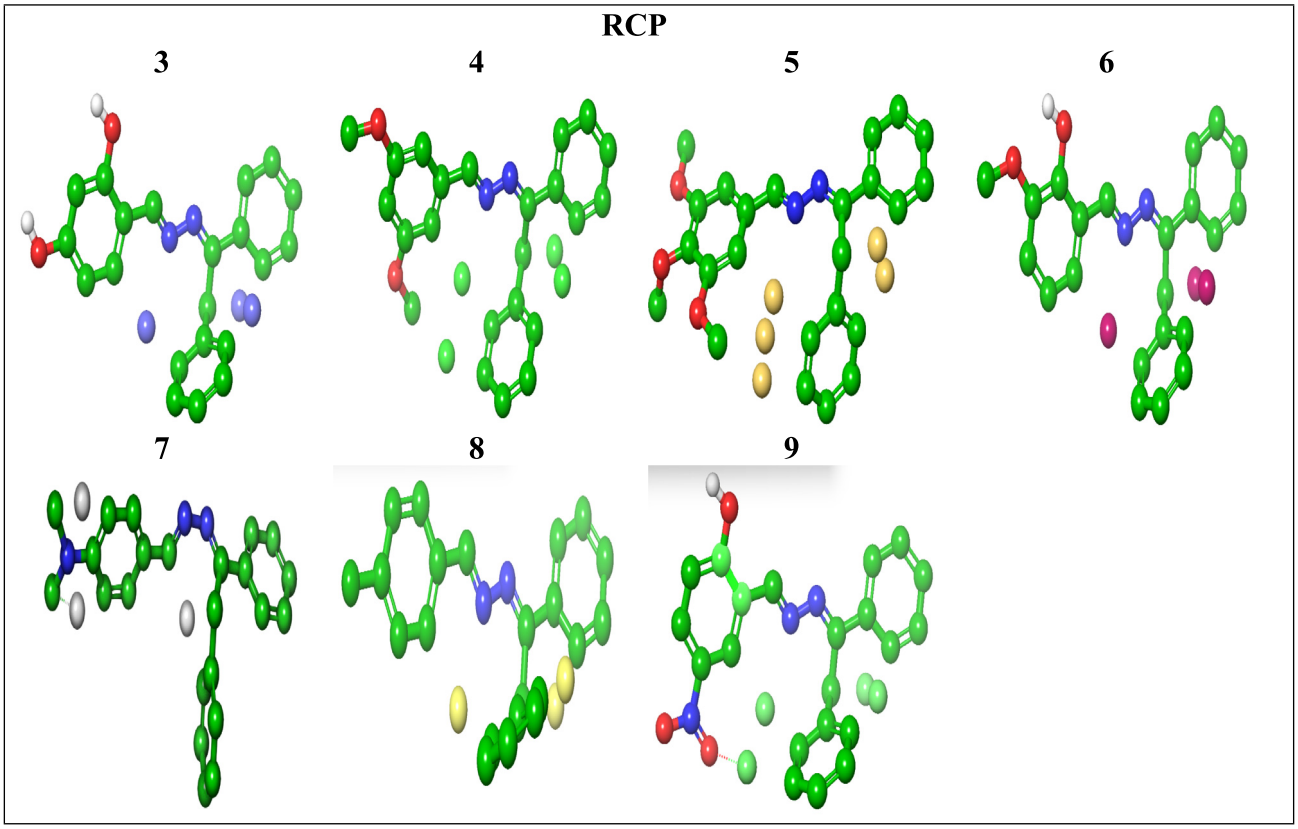

Fig. 6. BCP for **(3–9)** molecules from AIM theory.

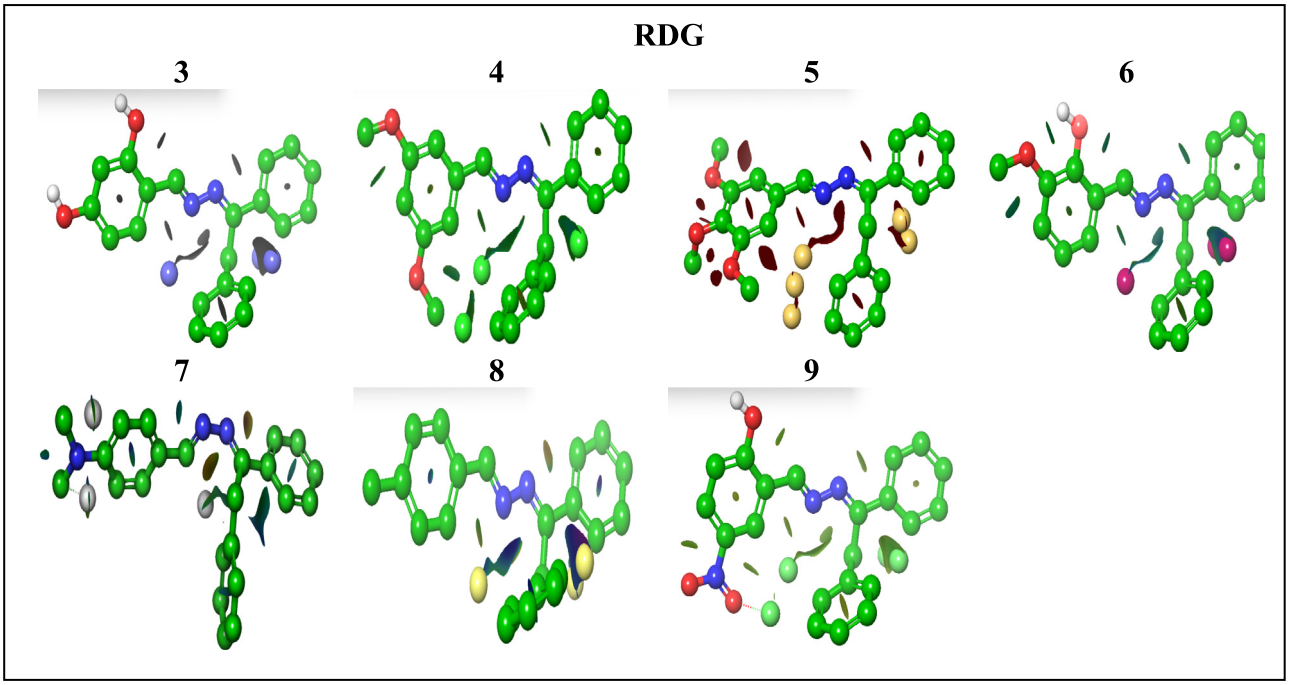

Fig. 7. RDG and NCI profile of **(3–9)** molecules using AIM theory.

values indicating hydrogen bonds, large positive values indicating repulsive interactions, and values close to zero indicating weak van der Waals interactions. In Fig. 7, molecules show the presence of strong hydrogen bonding between N-N for compounds **3** and **8** (blue isosurface sign $(\lambda_2)\rho$ value nearly -0.012) and weak van der Waals interactions (green isosurfaces) in compounds **4, 6** and

9. The red-coloured isosurface indicates steric repulsion present at compounds **5** and **7** with sign $(\lambda_2)\rho = 0.02$ (Kavimani et al., 2018).

4.7. Molecular docking

To understand how the three most active derivatives **3, 4** and **6** inhibits the urease enzyme, we performed molecular docking of the seven synthesised compounds **(3–9)** against its crystal urease (PDB: 4UBP) (Otero-De-La-Roza et al., 2012) complexed with "8-OXO-2-deoxyguanosine" as reference inhibitor. We used the most satisfactory docking conformations of all active compounds that were detected inside the active site with proper alignment. The active site consists of both hydrophilic (Arg 339, Asp 224, 363, 494, Glu 166, 223 and His 323, 324) and hydrophobic (Ala 170, 366, Cys 322, Lys 169, Leu 319, and Met 637) amino acids. These amino acids interact with the ligands of urease that are essential for its catalytic activity. We observed that almost all conformations of the ligands **(3–9)** had interactions with important residues inside the pocket.

The docking steps were applied as the previously reported method (Freudenthal et al., 2015, Irfan et al., 2023). We established the inhibition behaviour in binding-energy BE terms for seven tested compounds **(3–9)** with the receptors and compared the results with the reference inhibitor (**8-OD**). Compounds **(3–9)** redocked and achieved a root mean square deviation (RMSD) in range 1.2 and 1.9 Å (Table 3). Using the fingerprint interaction between ligand and protein (PLIF), binding effectiveness was assessed. The "Oples3e" molecular-mechanics force field created the poses. The pose with the lowest "E" and "RMSD" was chosen (Fig. 8) in order to evaluate the binding affinities of synthetic compounds **(3–9)**. For further validation of the molecular docking experiment ligand efficacy LE was calculated.

The binding mode and stability of the docked poses were evaluated by the Glide ΔG score, which estimates the free energy of binding between the ligand and the receptor protein.

The lowest score pose and RMSD is the more stable in the binding pocket. The data was used to rank the docked poses and to select the most capable docked conformation of each compound **(3–9)**. The docking energy details are shown in Table 3. The interactions between the seven active compounds **(3–9)** and the active site residues were mainly polar bonds, hydrogen bonding, $\pi - \pi$ and $\pi -$ H interactions, which contributed to a strong alignment with the enzyme backbone (Table 4).

Among seven investigated compounds **(3–9),** the most active three tested hybrids **3, 4** and **6** showed strong urease interactions (-6.25,-645 and −6.37, respectively), compared to other tested compounds **5, 7, 8** and **9,** while reference inhibitor stood out among them as having highest inhibitory activity with ΔG = −8.66 (Table 3).

The 1st and 2rd most active molecules **3** and **4** were attached deeply into the binding pockets, interacting with vital hydrophobic Ala170 residue. Compound **6** had the 3rd most active compound, although has lowest binding energies (-8.37 Kcal/mol) comforting in binding pocket by interacting with hydrophilic binding pocket Cys322 and Arg339, that led to decrees the activity against urease (Fig. 8). We believe it pinpoint of urease by formation strong interactions with important residues (Table 4). According to 3D-molecular docking the most active (benzylidene)-2-(1,2-diphenyle thylidene)hydrazine **3, 4** and **6** prefer a parallel orientation between phenyl ring and important hydrophobic Ala170. Docking revealed complicated interactions including strong hydrogen bonds with critical hydrophobic Ala170.

4.8. Molecular dynamic investigations of the most bioactive 3, 4 and 6 molecules

It is unsuitable for explaining the interaction between the molecular docking calculations and the ligand–protein at the ns level, although the ligand molecules are pretty flexible in the calculations. In Molecular Mechanics-Poisson-Boltzmann surface area (MM-PSBA) calculations as implemented in molecular dynamic, the interaction between ligand and urease enzyme is done at the 250 ns. Both ligand molecule and urease protein have flexibility in calculations of (MM-PSBA). The interaction occurring in these calculations is examined every 2 ns, and the energy change is given in Fig. 9.

The resulting graph shows the binding free energy changes and deviations in each ten (ns) interval in Fig. 9. The energy changes of the most active three most active compounds **3, 4** and **6** molecules were compared with each other. With this comparison, calculations were made to support the estimation of the free energies of the bonding using the molecular MMPBSA method. The negative value of the relevant parameters indicates better binding (Aktaş and Yüksel, 2020). The results were calculated using equation-1. Furthermore, the slight deviation for MM-PBSA for **3, 4** and **6** complexed with urease over-all time-scale, figured that strong interaction between Ligand and amino acids backbone, which showed a firm H-bonding pattern.

4.9. In-Silico toxicological study

4.9.1. In-Silico pharmacokinetic profile

In-Silico cytotoxicity screening through ADMET (absorption, distribution, metabolism, and excretion toxicity) parameters acting a fundamental route in therapeutic bioactive molecules **(3–9)** were carried out. SwissADME (Daina et al., 2017) and ADMET-SAR model were used to predict parameters for seven investigated molecules **(3–9)**, which these disclosed in (Table 5).

The physicochemical and ADMET parameters stated that these ligands are suitable for all investigated rules as Lipinski, Ghose, Veber, Egan, Muegge rules with no violations. All seven investigated compounds **(3–9)** were authorization to Lipinski, Ghose

Table 3
The binding-affinity energies in kcal/mol of **(3–9)** and 8OD against urease enzyme.

C. No	ΔG	RMSD	H. B	EInt.	Eele	LE
3	−6.287	1.489	33.852	−5.811	−4.821	−29.623
4	−6.454	1.405	27.058	−8.212	−8.446	−30.980
5	−7.293	1.957	55.464	−7.699	−6.124	−41.403
6	−6.375	1.471	53.983	−5.793	−6.368	−36.588
7	−6.020	1.905	78.305	−5.419	−5.486	−20.602
8	−6.383	1.261	62.538	−2.728	−5.957	−36.394
9	−5.920	1.746	44.762	−6.125	−6.075	−27.983
8-OD	−8.660	1.200	−214.387	−5.803	−9.493	−311.345

Where, *ΔG*: Free binding energy of the ligand; RMSD: root-mean-square deviation; *H.B.*: H-bonding energy between protein and ligand; EInt: Binding affinity of H-bond interaction with receptor; Eele: Electrostatic interaction over the receptor.

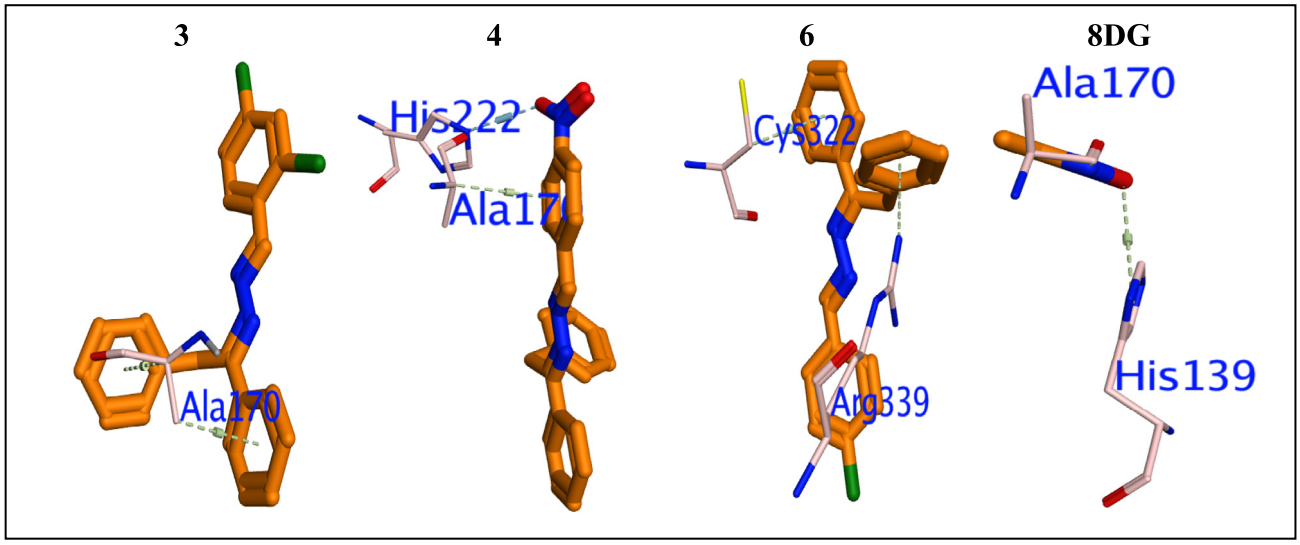

Fig. 8. 3D mapping surface of three most active compounds **3, 4** and **6** with reference 8-Oxo-2′-deoxyguanosine inside the urease active site 4UBB.

Table 4
Interaction details of compounds **(3–9)** and **8-OD.**

	Ligand		Receptor		Interaction	Distance(A°)	E(kcal/mol)
3	6-ring	CA	ALA	170	π-H	3.93	−0.7
	6-ring	CB	ALA	170	π-H	3.66	−0.7
4	O38	NE2	HIS	222	H-acceptor	3.17	−2
	6-ring	CA	ALA	170	π-H	4.05	−0.9
5	O43	NE2	HIS	222	H-acceptor	2.91	−3.6
	O43	NI	NI	798	Metal	2.59	−0.8
	6-ring	CB	GLU	166	π-H	4.22	−0.5
6	6-ring	CB	CYS	322	π-H	4.07	−0.7
	6-ring	NH2	ARG	339	π-cation	3.79	−0.5
7	S41	OD1	ASP	363	H-donor	4.07	−1
	S41	OD2	ASP	363	H-donor	4.12	−1.1
	C17	5-ring	HIS	324	π-H	4.01	−0.5
	6-ring	CA	ALA	170	π-H	4.13	−0.7
8	C23	5-ring	HIS	324	π-H	3.77	−1.1
	6-ring	CA	ALA	170	π-H	4.06	−1.2
9	6-ring	CA	ALA	170	π-H	4.15	−0.8
8-OD	N8	O	ALA	170	H-donor	3.43	−1.1
	N9	NI	NI	798	Ionic	3.09	−3.9
	N10	NI	NI	799	Ionic	2.81	−5.9
	O10	NI	NI	798	Ionic	2.46	−9.3
	O11	NI	NI	799	Ionic	2.23	−12.3
	O12	5-ring	HIS	139	π-cation	4.79	−0.9

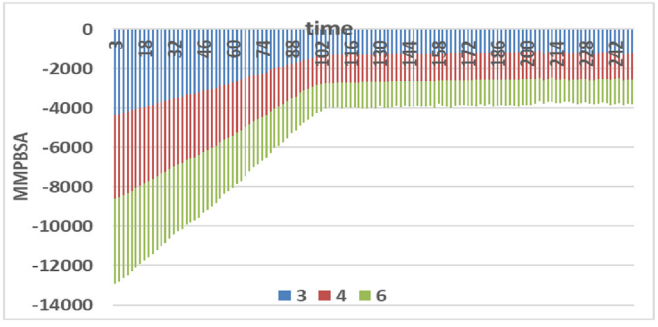

Fig. 9. Display the Gibbs free energy values of protein and ligand molecules every ten ns intervals.

and Muegge rules, and pass *via* Veber, Egan with one violation related to TPSA. Consequently, the tested compound **(3–9)** exhibited promising bioavailability scores (0.55).

The data presented by **(3–9)** compounds confirmed that molecules are promising oral bioavailability without affected by biodegradation. The Bioavailability Radar for analysis of drug-likeness was represented in (Fig. 8). The relationship between polarity, size, liphophilicity, solubility, saturation, and flexibility was presented by the reader (Ritchie et al., 2011), pink color characterized the ideal ranges for each features.

The reader of **(3–9)** showed no deflection against any parameters **(**Fig. 9**)**. Seventh compound had low Csp3 Fraction values ranging from 0.05 to 0.09 (passing value Csp3 < 0.25) (Zhao et al., 2002), which indicate a low degree of saturation of the carbon atoms. Another important factor for absorption in silico is water solubility (Zhao et al., 2015), which these compounds exhibited strongly absorption. Using ADMET-SAR pharmacokinetic characteristics, mutagenic, tumorigenic, reproductively effective, irritant, and human intestinal absorption were examined in silico (Banerjee et al., 2018). Furthermore, another support vector machine algorithm was applied to identify substrates or non-substrates of the permeability for skin permeation (Log Kp), Caco-2, blood brain bar-

Table 5
In-silico ADMET and drug likeness for seven investgate compounds **(3–9).**

	3	4	5	6	7	8	9
MW	367.27	343.38	359.38	332.83	344.47	312.41	314.38
Fraction Csp3	0.05	0.05	0.05	0.05	0.09	0.09	0.05
H-bond acceptors	2	4	5	2	2	2	3
H-bond donors	0	0	1	0	0	0	1
MR	107.39	106.19	108.21	102.38	109.09	102.33	99.39
TPSA	24.72	70.54	90.77	24.72	50.02	24.72	44.95
iLOGP	3.96	3.14	2.59	3.78	3.76	3.84	3.12
XLOGP3	6.37	4.94	4.59	5.74	5.62	5.48	4.76
Consensus Log P	5.81	4.15	3.54	5.3	5.28	5.11	4.34
ESOL Log S	−6.33	−5.2	−5.06	−5.74	−5.65	−5.45	−5.01
Ali Log S	−6.68	−6.16	−6.22	−6.03	−6.43	−5.76	−5.43
GI absorption	High	High	High	High	High	High	High
BBB permeant	No	Yes	No	Yes	Yes	Yes	Yes
Pgp substrate	Yes	No	No	Yes	Yes	Yes	No
CYP1A2 inhibitor	Yes	Yes	No	Yes	Yes	Yes	No
CYP2C19 inhibitor	Yes	Yes	Yes	Yes	Yes	Yes	Yes
CYP2C9 inhibitor	No	No	Yes	No	No	No	No
CYP2D6 inhibitor	No	No	No	No	No	No	No
CYP3A4 inhibitor	No	No	No	No	No	No	No
log Kp (cm/s)	−4.02	−4.89	−5.23	−4.25	−4.41	−4.31	−4.84
Lipinski #violations	1	1	0	1	1	1	0
Ghose #violations	1	0	0	0	0	0	0
Veber #violations	0	0	0	0	0	0	0
Egan #violations	1	0	0	0	0	0	0
Muegge #violations	1	0	0	1	1	1	0
Bioavailability Score	0.55	0.55	0.55	0.55	0.55	0.55	0.55
PAINS #alerts	0	0	1	0	0	0	1
Brenk #alerts	1	3	3	1	1	1	1
Carcinogenicity	0.767	0.871	0.904	0.772	0.882	0.812	0.849
hERG	0.011	0.032	0.019	0.01	0.011	0.007	0.009
Pgp-inh	0.113	0.023	0.045	0.069	0.155	0.306	0.254
Pgp-sub	0.002	0.003	0.003	0.002	0.004	0.006	0.005
IGC_{50}	5.253	4.97	5.132	5.055	5.031	4.973	5.031
LC_{50}	6.919	6.711	6.592	6.642	6.583	6.311	6.309

rier (BBB) and p-glycoprotein (P-gp), as well as, to recognize inhibition effects against the main cytochromes P450 isoenzymes (CYP1A2, CYP2C19, CYP2C9, CYP2D6, and CYP3A4). The results obtained from (Table 5) showed that these compounds did not have the ability to inhibit any types of P450.

The compounds **(3–9)** in this study have low (Log Kp) and Caco-2 values, indicating low permeability across skin and intestinal cells. The Boiled-Egg model can be used to visualize the relationship between WLOGP and TPSA (Fig. 10), which shows that the compounds have high BBB permeability, high GI absorption, high brain penetration, weak inhibition of (hERG) in the range of (0.01–0.03) and no resistance to P-gp protein. Compounds do not exhibit carcinogenicity, mutagenicity or tumorigenicity when compared with 981 carcinogenic chemicals from the "Carcinogenic Potency Database (CPDB)" (Lowry et al., 1951).

4.9.2. Oral toxicity prediction

We used the Chemical European Biology Laboratory (ChEMBL) database to forecast the potential toxicity of seven molecules in this study by examining the assessment of oral rodents on an extracted basis. We also estimated the lower lethal doses (LD_{50}) values in rodents and found that our ligands have significant LD_{50} (4.9–5.2) compared. We based our toxicity calculation on the highest endpoints of 33 models (Table 5). We divided the calculated schematic into several stages of toxicity, such as toxicity, toxicological endpoints (mutagenicity, carcino toxicity, organ toxicity (hepatotoxicity), cytotoxicity and immuno toxicity), toxicological pathways (AOPs) and toxicity targets. This approach gave us a suitable insight into the possible molecular mechanism and toxic response.

5. Conclusion

Novel *bis*-Schiff base derivatives based on benzyl phenyl ketone nucleus was successfully synthesized and characterized with FTIR, HR-ESI-MS and ^{1}H NMR spectroscopy. These compounds were finally screened for *in vitro* urease inhibition activity. All the synthesized derivatives **(3–9)** showed excellent to less inhibitory potential when compared with standard thiourea (IC_{50} = 21.15 ± 0.32 μM). The most potent derivatives among the series are compounds **3** (IC_{50} = 22.21 ± 0.42 μM), **4** (IC_{50} = 26.11 ± 0.22 μM) and **6** (IC_{50} = 28.11 ± 0.22 μM) near to standard thiourea. In the same way, compound **5** having IC_{50} value of 34.32 ± 0.65 μM was showed significant inhibitory activity while three compounds **7, 8,** and **9** exhibited less activity with IC_{50} values of 45.91 ± 0.14, 47.91 ± 0.14, and 48.33 ± 0.72 μM respectively. DFT expanded on **3–9** molecules to calculate FMO, which indicating that these molecules are stable, have a bioactive nature, and experienced charge transfer. MEP visual the reactive regions of **3–9** molecules, these regions are close to the ═N—N═ atoms and its more electrophilic and can interact with protein receptors. The AIM-topological investigation of **3–9** demonstrated that the H-bond energy is minimal and that the interactions are non-covalent. ELF applied to investigate the electron-localization-degree. The molecular docking showed the most active compounds **3, 4** and **6** are binding with the same manner with of reference inhibitor. MD over 250 ns figured that strong interaction between most active **3, 4** and **6**

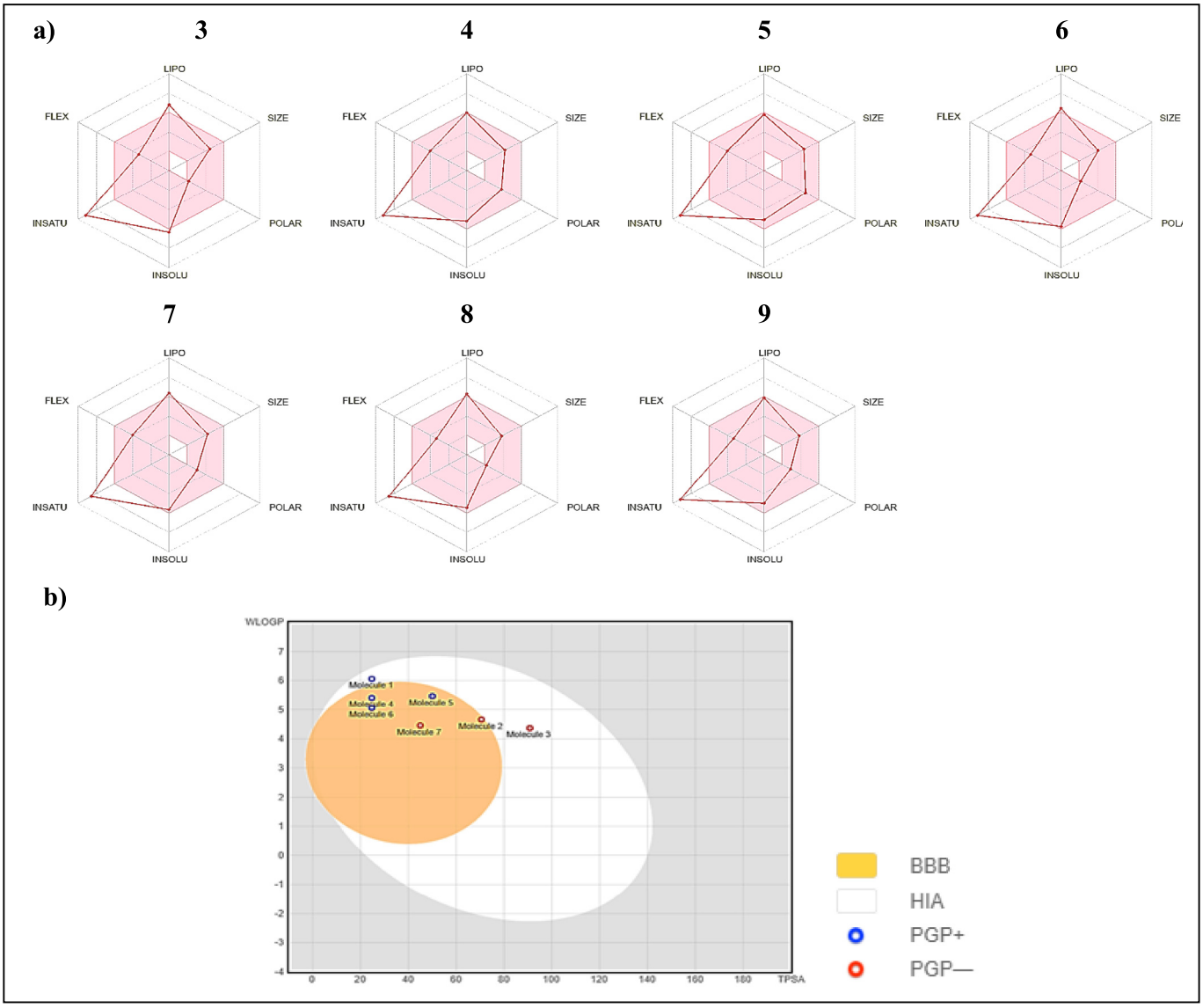

Fig. 10. **a**) The optimal range as red color for; Lipophilicity: −0.7 ≤ XLOGP3 ≤ +5.0, size: 150 ≤ MW ≤ 500 g/mol, polarity: TPSA ≤ 140 Å2, solubility: log S ≤ 6, saturation fraction of carbons in the hybridization sp3 ≥ 0.25, and flexibility: rotatable bonds ≤ 9. **b**) BOILED-Egg plot, White and yellow color represented highly probable for HIA (GI) absorption and BBB permeation, respectively, grey outside for molecules are low absorption and not brain penetration, blue and red points represented as P-gp substrate (PGP +) and P-gp non-substrate (PGP −), respectively.

molecules and vital amino acids backbone. ADMET showed that **3**–**9** compounds do not exhibit carcinogenicity, mutagenicity or tumorigenicity.

Declaration of Competing Interest

The authors declare that they have no known competing financial interests or personal relationships that could have appeared to influence the work reported in this paper.

Acknowledgement

Authors are thankful to researchers supporting project number (RSP2023R335), King Saud University, Riyadh, Saudi Arabia.

References

Abdelmadjid, A., Haffar, D., Benghanem, F., Ghedjati, S., Toukal, L., Dorcet, V., Bourzami, R., 2021. Synthesis, crystal structure, electrochemical, theoretical studies and antioxidant activities of new Schiff base. J. Mol. Struct. 1227, 129368.

Ahmad, S., Khan, M., Shah, M.I.A., Ali, M., Alam, A., Riaz, M., Khan, K.M., 2022. Synthetic Transformation of 2-{2-Fluoro [1, 1′-biphenyl]-4-yl} Propanoic acid into hydrazide-hydrazone derivatives. In vitro urease inhibition and in silico study. ACS Omega 7, 45077–45087.

Ahmed, M., Qadir, M.A., Hameed, A., Arshad, M.N., Asiri, A.M., Muddassar, M., 2017. Azomethines, isoxazole, N-substituted pyrazoles and pyrimidine containing curcumin derivatives: urease inhibition and molecular modeling studies. Biochem. Biophys. Res. Commun. 490, 434–440.

Aktaş, T., Yüksel, O., 2020. Effects of vermicompost on aggregate stability, bulk density and some chemical characteristics of soils with different textures. Tekirdağ Ziraat Fakültesi Dergisi 17, 1–11.

Alam, A., Ali, M., Latif, A., Rehman, N.U., Saher, S., Khan, A., Ullah, S., Ullah, O., Halim, S.A., Sani, F., 2022a. Novel Bis-Schiff's base derivatives of 4-nitroacetophenone as potent α-glucosidase agents: design, synthesis and in silico approach. Bioorg. Chem. 128, 106058.
Alam, A., Ali, M., Rehman, N.U., Ullah, S., Halim, S.A., Latif, A., Khan, A., Ullah, O., Ahmad, S., Al-Harrasi, A., 2022b. Bio-Oriented synthesis of novel (S)-Flurbiprofen clubbed hydrazone Schiff's bases for diabetic management. In vitro and in silico studies. Pharmaceuticals 15, 672.
Al-Mudhafar, M.M.J., Omar, T.N., Abdulhadi, S.L., 2022. Bis-Schiff bases of isatin derivatives synthesis, and their biological activities: a review. Al Mustansiriyah J. Pharm. Sci. 22, 23–48.
Arshad, I., Saeed, A., Channar, P.A., Shehzadi, S.A., Ahmed, M.N., Siddiq, M., 2020. Bis-Schiff bases of 2, 2′-dibromobenzidine as efficient corrosion inhibitors for mild steel in acidic medium. RSC Adv. 10, 4499–4511.
Banerjee, P., Eckert, A.O., Schrey, A.K., Preissner, R., 2018. ProTox-II: a webserver for the prediction of toxicity of chemicals. Nucleic Acids Res. 46, W257–W263.
Cantarella, H., Otto, R., Soares, J.R., de Brito Silva, A.G., 2018. Agronomic efficiency of NBPT as a urease inhibitor: a review. J. Adv. Res. 13, 19–27.
Costa, R.A., Pitt, P.O., Pinheiro, M.L.B., Oliveira, K.M., Salomé, K.S., Barison, A., Costa, E.V., 2017. Spectroscopic investigation, vibrational assignments, HOMO-LUMO, NBO, MEP analysis and molecular docking studies of oxoaporphine alkaloid liriodenine. Spectrochim. Acta A Mol. Biomol. Spectrosc. 174, 94–104.
Daina, A., Michielin, O., Zoete, V., 2017. SwissADME: a free web tool to evaluate pharmacokinetics, drug-likeness and medicinal chemistry friendliness of small molecules. Sci. Rep. 7, 42717.
Domingo, L. RSC Adv. 2014, 4, 32415-32428. https://doi.org/10.1039/C4RA04280H.
Domínguez, M.J., Sanmartín, C., Font, M., Palop, J.A., San Francisco, S., Urrutia, O., Houdusse, F., García-Mina, J.M., 2008. Design, synthesis, and biological evaluation of phosphoramide derivatives as urease inhibitors. J. Agric. Food Chem. 56, 3721–3731.
Figueredo, A.S., Queiroz, J.E., Dias, L.D., Vidal, H.D., Machado, I.V., Vila Verde, G.M., Aquino, G.L., 2019. Synthesis and anticholinesterase activity evaluation of asymmetric azines. Pharm. Chem. J. 53, 544–549.
Freudenthal, B.D., Beard, W.A., Perera, L., Shock, D.D., Kim, T., Schlick, T., Wilson, S. H., 2015. Uncovering the polymerase-induced cytotoxicity of an oxidized nucleotide. Nature 517, 635–639.
Frisch, M., Trucks, G., Schlegel, H., Scuseria, G., Robb, M. & Cheeseman, J. 2010. Gaussian 09, C3 Revision B. 01. Gaussian Inc, Walling-form CT.
Irfan, A., Faisal, S., Ahmad, S., Al-Hussain, S.A., Javed, S., Zahoor, A.F., Parveen, B., Zaki, M.E., 2023. Structure-Based Virtual Screening of Furan-1, 3, 4-Oxadiazole Tethered N-phenylacetamide Derivatives as Novel Class of hTYR and hTYRP1 Inhibitors. Pharmaceuticals 16, 344.
Kafarski, P., Talma, M., 2018. Recent advances in design of new urease inhibitors: a review. J. Adv. Res. 13, 101–112.
Kavimani, M., Balachandran, V., Narayana, B., Vanasundari, K., Revathi, B., 2018. Topological analysis (BCP) of vibrational spectroscopic studies, docking, RDG, DSSC, Fukui functions and chemical reactivity of 2-methylphenylacetic acid. Spectrochim. Acta A Mol. Biomol. Spectrosc. 190, 47–60.
Khan, M., Alam, A., Khan, K.M., Salar, U., Chigurupati, S., Wadood, A., Ali, F., Mohammad, J.I., Riaz, M., Perveen, S., 2018. Flurbiprofen derivatives as novel α-amylase inhibitors: biology-oriented drug synthesis (BIODS), in vitro, and in silico evaluation. Bioorg. Chem. 81, 157–167.
Khan, K.M., Khan, M., Ali, M., Taha, M., Rasheed, S., Perveen, S., Choudhary, M.I., 2009. Synthesis of bis-Schiff bases of isatins and their antiglycation activity. Bioorg. Med. Chem. 17, 7795–7801.
Kosikowska, P., Berlicki, Ł., 2011. Urease inhibitors as potential drugs for gastric and urinary tract infections: a patent review. Expert Opin. Ther. Pat. 21, 945–957.
Lowry, O.H., Rosebrough, N.J., Farr, A.L., Randall, R.J., 1951. Protein measurement with the Folin phenol reagent. J. Biol. Chem. 193, 265–275.
Lu, T., Chen, F., 2012. Multiwfn: a multifunctional wavefunction analyzer. J. Comput. Chem. 33, 580–592.
Nasli-Esfahani, E., Mohammadi-Khanaposhtani, M., Rezaei, S., Sarrafi, Y., Sharafi, Z., Samadi, N., Faramarzi, M.A., Bandarian, F., Hamedifar, H., Larijani, B., 2019. A new series of Schiff base derivatives bearing 1, 2, 3-triazole: design, synthesis, molecular docking, and α-glucosidase inhibition. Arch. Pharm. 352, 1900034.
Okoli, B.J., Modise, J.S., 2018. Investigation into the thermal response and pharmacological activity of substituted Schiff Bases on α-Amylase and α-Glucosidase. Antioxidants 7, 113.
Otero-De-la-roza, A., Johnson, E.R., Contreras-García, J., 2012. Revealing non-covalent interactions in solids: NCI plots revisited. PCCP 14, 12165–12172.
Rahim, F., Zaman, K., Taha, M., Ullah, H., Ghufran, M., Wadood, A., Rehman, W., Uddin, N., Shah, S.A.A., Sajid, M., 2020. Synthesis, in vitro alpha-glucosidase inhibitory potential of benzimidazole bearing bis-Schiff bases and their molecular docking study. Bioorg. Chem. 94, 103394.
Ritchie, T.J., Ertl, P., Lewis, R., 2011. The graphical representation of ADME-related molecule properties for medicinal chemists. Drug Discov. Today 16, 65–72.
Silva, A.G., Sequeira, C.H., Sermarini, R.A., Otto, R., 2017. Urease inhibitor NBPT on ammonia volatilization and crop productivity: a meta-analysis. Agron. J. 109, 1–13.
Soares, J.R., Cantarella, H., de Campos Menegale, M.L., 2012. Ammonia volatilization losses from surface-applied urea with urease and nitrification inhibitors. Soil Biol. Biochem. 52, 82–89.
Sudkolai, S.T., Nourbakhsh, F., 2017. Urease activity as an index for assessing the maturity of cow manure and wheat residue vermicomposts. Waste Manage. 64, 63–66.
Ullah, H., Rahim, F., Taha, M., Hussain, R., Tabassum, N., Wadood, A., Nawaz, M., Mosaddik, A., Imran, S., Wahab, Z., 2020. Aryl-oxadiazole Schiff bases: Synthesis, α-glucosidase in vitro inhibitory activity and their in silico studies. Arab. J. Chem. 13, 4904–4915.
Upadyaya, S., Bhagavath, P., Sunil, D., 2018. Azines as liquid crystalline materials: an up-to-date review. J. Mol. Liq. 269, 354–370.
Yapar, G., Demir, N., Kiraz, A., Özkat, G.Y., YıLDıZ, M., 2022. Synthesis, biological activities, antioxidant properties, and molecular docking studies of novel bis-schiff base podands as responsive chemosensors for anions. J. Mol. Struct. 133530.
Zainab, YuH., Rehman, N.U., Ali, M., Alam, A., Latif, A., Shahab, N., Amir Khan, I., Jabbar Shah, A., Khan, M., Al-Ghafri, A., 2022. Novel Polyhydroquinoline-Hydrazide-Linked Schiff's base derivatives: multistep synthesis, antimicrobial, and calcium-channel-blocking activities. Antibiotics 11, 1568.
Zhao, Y.H., Abraham, M.H., Le, J., Hersey, A., Luscombe, C.N., Beck, G., Sherborne, B., Cooper, I., 2002. Rate-limited steps of human oral absorption and QSAR studies. Pharm. Res. 19, 1446–1457.
Zhao, Y., Zheng, X., Zhang, H., Zhai, J., Zhang, L., Li, C., Zeng, K., Chen, Y., Li, Q., Hu, X., 2015. In vitro inhibition of AKR1Cs by sulphonylureas and the structural basis. Chem. Biol. Interact. 240, 310–315.
Zhong, X., Yi, J., Sun, J., Wei, H.-L., Liu, W.-S., Yu, K.-B., 2006. Synthesis and crystal structure of some transition metal complexes with a novel bis-Schiff base ligand and their antitumor activities. Eur. J. Med. Chem. 41, 1090–1092.